

A FRAMEWORK FOR UNDERSTANDING THE BIOCONCENTRATION OF SURFACTANTS IN FISH

Michael S. McLachlan¹, Andrea Ebert², James M. Armitage³, Jon A. Arnot^{4,5} and Steven T. J. Droge⁶

¹Department of Environmental Science, Stockholm University, 106 91 Stockholm, Sweden

²Department of Analytical Environmental Chemistry, Helmholtz Centre for Environmental Research - UFZ, D-04318 Leipzig, Germany

³AES Armitage Environmental Sciences, Inc., Ottawa, Ontario K1L 8C3, Canada

⁴ARC Arnot Research and Consulting Inc., Toronto, Ontario M4M 1W4, Canada

⁵Department of Physical and Environmental Sciences, University of Toronto Scarborough, Toronto, Ontario M1C 1A4, Canada

⁶Wageningen Environmental Research, team Environmental Risk Assessment, 6700 AA Wageningen, The Netherlands

E-mail contact: michael.mclachlan@aces.su.se

SUPPORTING INFORMATION

Table of Contents

Text		
S1	Lateral transport	S2
S2	Solubility diffusion model	S3
S3	Parameterization of the framework	S5
Figures		
S1	Illustration of the 4-resistance model of surfactant exchange across the gills	S6
S2	Fit of model to observations for cationic surfactants, recalculated from Kierkegaard et al.	S7
S3	Model vs. measured k_T for cationic surfactants (including biotransformation).	S10
Tables		
S1	Selected nonionic surfactants with tonnage >1000/y in the EU	S11
S2	Selected zwitterionic surfactants with tonnage >1000/y in the EU	S11
S3	Kinetic parameters for cationic surfactants recalculated from Kierkegaard et al.	S12

Text S1: Lateral transport

As shown in Figure S1, lateral transport is the movement of chemical through the epithelium within the cell membrane. In Bittermann and Goss (2017), no significant lateral transport was assumed for ionic compounds. However, this assumption could not be verified with the dataset in that study because other resistances such as the permeation through the unstirred water layer dominated the Caco-2 (human colorectal adenocarcinoma cells) and MDCK (Madin-Darby canine kidney cells) cell permeation. With the dataset of Ribbenstedt et al. (2022) on anionic surfactants, on the other hand, we are now able to analyze the significance of the lateral transport for ions more clearly. When we calculated lateral transport for ionic compounds using the equations presented in Bittermann and Goss (2017) for neutral compounds, modeled cell permeation, and as a consequence uptake rate constants k_u , were clearly overestimated compared to experimental k_u . Lateral permeation of ions can thus clearly not be calculated analogously to neutral compounds. Therefore, in the absence of a calculation method for ionic compounds we still assume no significant lateral transport.

Although lateral transport for neutral chemicals was also deemed irrelevant in Bittermann and Goss (2017), these findings cannot automatically be assumed to apply to our current application, because the dataset contained compounds that are less hydrophobic and the transwell setups for Caco-2 and MDCK cells exhibit much thicker unstirred water layers (>300 μm) than gills in fish (a few μm). The more hydrophobic compounds, for which lateral transport might potentially play a role, were thus not limited by the epithelial monolayer resistances in the Caco-2/ MDCK experiments, but by the resistance of the unstirred water layer. Hence no information about the magnitude of the lateral transport (or any other monolayer resistance) of hydrophobic chemicals can be obtained from the Caco-2/ MDCK experiments.

Lateral transport per se can only be relevant when the transport through the cytosol is rate limiting, since membrane permeability itself exceeds lateral permeability due to the lesser space available for lateral diffusion. We assume aqueous resistances (including the cytosol resistance) to be insignificant compared to the resistance for delivery of the water to the gills (see section "Mass transfer across gills"). Consequently, even if lateral permeation should exceed transcellular permeability for very hydrophobic compounds, the resistance of the cell monolayer as a whole would be insignificant. Therefore, lateral transport does not need to be included in the framework.

Text S2: Solubility-diffusion model

The solubility-diffusion model describes membrane permeation as the partitioning into and the diffusion through the membrane. Hereby, the anisotropy of the membrane has to be considered: The partitioning into the region of polar headgroups will differ from the partitioning into the hydrocarbon membrane core. Although the partitioning into the most favorable layers of the membrane will be crucial for the K_{MLW} or D_{MLW} , the partitioning into the least favorable layers will decide membrane permeability, since the latter dominates the total membrane resistance. For the compounds of interest here, it can be assumed that the membrane core provides the highest barrier to permeation. Thus, for a simplified calculation the membrane is often approximated as a thin slab of apolar solvent such as hexadecane, which has a dielectric constant similar to the membrane core. The intrinsic permeability $P_{M,n}$ of the neutral species can thus be calculated as follows (Missner and Pohl, 2009):

$$P_{M,n} = \frac{D_m \times K_{hex/w}}{d} \quad (S1)$$

where D_m is the diffusion coefficient in the membrane core, which is assumed reduced by a factor of 10 as compared to water (Orbach and Finkelstein, 1980), $K_{hex/w}$ is the hexadecane/water partition coefficient, and d the thickness of the membrane core.

The permeability also correlates with octanol/water partition coefficient K_{OW} , and although the correlation is not as good as for hexadecane, we will use the following correlation found by Walter and Gutknecht (1986) to predict neutral intrinsic permeability $P_{M,n}$ (cm s^{-1}):

$$\log(P_{M,n}) = 1.15 \times \log(K_{OW}) - 2.14 \quad (S2)$$

Combining this correlation with an empirical correlation relating the K_{MLW} to the K_{OW} (Endo et al., 2011; see Eq. S3) leads then to the correlation between $P_{M,n}$ and the K_{MLW} expressed in Eq. S4:

$$\log(K_{MLW}) = 1.01 \times \log(K_{OW}) + 0.12 \quad (S3)$$

$$\log(P_{M,n}) = 1.14 \times \log(K_{MLW}) - 2.28 \quad (S4)$$

To reduce the number of variables in the framework, we use the D_{MLW} in the correlation instead of the K_{MLW} . Expressed in non-logarithmic form, the used correlation reads as follows:

$$P_{M,n} = 0.00525 \times D_{MLW}^{1.14} \quad (S5)$$

Converting the units for $P_{M,n}$ to m h^{-1} yields:

$$P_{M,n} = 0.189 \times D_{MLW}^{1.14} \quad (S6)$$

It is important to acknowledge assumptions and approximations in this approach that can contribute significant uncertainty:

- Approximating the partitioning into the membrane core with K_{OW} instead on $K_{hex/w}$. As noted above, octanol is not as strong a model for the partitioning properties of the membrane core as hexadecane.
- Using D_{MLW} to approximate K_{MLW} . The D_{MLW} of ionic compounds is expected to be lower than the neutral K_{MLW} . Nevertheless, we expect them to be quite strongly correlated with each other.

- Approximating $P_{M,n}$ for biological membranes with measurements made using black lipid membranes (BLM, in which the measurements of Walter and Gutknecht were made). Permeability in biological membranes is considerably lower than in BLM (Lomize and Pogozheva, 2019).

We note that while each of these factors can contribute considerably to the uncertainty of $P_{M,n}$ for a given compound, their influence on the relative value of $P_{M,n}$ for compounds with similar structures such as hydrocarbon anionic surfactants (the compounds for which $P_{M,n}$ is relevant in our framework) is anticipated to be less pronounced. Furthermore, the second and third factors above are expected to partially cancel each other out. Finally, as the comparison to empirical data for anionic surfactants in the paper shows, the uncertainty in pK_a for anionic surfactants is currently so great that the absolute value of $P_{M,n}$ could not be employed in the framework; instead it was used to estimate the pK_a . As such, the absolute value of $P_{M,n}$ is of limited importance for current application of the framework. However, as better estimates of pK_a for anionic surfactants become available and understanding of cell membrane permeability improves, there will be opportunities to further develop this aspect of the framework.

We further assume that the permeation is governed by the neutral species alone, i.e., that ionic permeation is insignificant and only the neutral form contributes to this aspect of the transcellular pathway (see Figure S1 below). Although this assumption is commonplace, it might be questionable for some ionic surfactants which due to their very low pK_a exist predominantly in their ionic form. On the other hand, intrinsic ionic permeability is usually orders of magnitude lower than intrinsic neutral permeability, because it is energetically very unfavorable to bring the charge from water into the membrane core. To assess the validity of our assumption, we used COSMOtherm (Eckert and Klamt, 2004; Bittermann and Goss, 2017; Ebert et al., 2018) to calculate neutral and ionic permeability and pK_a values for selected surfactants: the anionic surfactants from Ribbenstedt et al. ($n = 11$), dodecyl hydrogen phosphate and 2-ethylhexyl phosphate. For all these surfactants, the calculations showed that the neutral permeation is still dominant. This is, however, not always the case: According to previous calculations of neutral permeability and pK_a , and experimental measurements of the ionic permeability, perfluorooctanesulfonic acid (PFOS) dissociates so strongly that ionic permeation should clearly dominate, while for perfluorooctanoic acid (PFOA) both the neutral and ionic species might be relevant (Ebert et al., 2020). This is in line with a recent report showing only a weak pH dependence of k_U for the uptake of PFOA in carp (Dong et al., 2023). For many ionizable surfactants our generalized approach will be valid, but for anionic surfactants with very low pK_a values the assumption that only the neutral species permeates the membrane via the transcellular pathway may need to be revisited.

As discussed in the main text, the framework predicts that paracellular transport dominates the uptake of permanently charged quaternary ammonium-based surfactants (QACs) across the gills. Accordingly, the solubility-diffusion model and its assumptions are not relevant and the uptake kinetics of all such compounds are expected to be similar. Although the bioaccumulation potential of Q14 is not of regulatory concern ($BCF = 54$ L/kg; see Table S3), it would still be useful to confirm or refute the predictions of the framework for a series of QACs spanning a range of $\log D_{MLW}$ values. For example, a positive relationship between k_U and D_{MLW} for QACs would not be consistent with the framework as currently formulated.

Text S3: Parameterization of the framework

Parameter	Abb.	Value	Unit	Source
Fish mass	M	0.01	kg	Assumed. BCF experiments commonly use fish with approximately this mass.
Gill surface area	A_{Gill}	0.0027	m ²	Correlation from Hughes (1984) for <i>Salmo gairdneri</i> , calculated for a 10 g fish.
Water flow through gills	$Q_{\text{W,Gill}}$	0.000264	m ³ h ⁻¹	Correlation from Arnot and Gobas (2004), calculated for a 10 g fish and an O ₂ concentration in water of 11.1 mg L ⁻¹ .
Blood flow rate through gills	$Q_{\text{B,Gill}}$	0.0000226	m ³ h ⁻¹	Correlation for rainbow trout from Erickson et al. (2006), calculated for a 10 g fish at 10 °C.
Fraction of membrane lipids in blood	$f_{\text{M-Lipid,B}}$	0.007	kg L ⁻¹	50% of the lipid of rainbow trout blood reported by Bertelsen et al. (1998).
Permeability for paracellular transport	P_{Paracell}	0.000161	m h ⁻¹	See below.

For small molecules, the paracellular resistance $R_{\text{P,W} \rightarrow \text{B}}$ is not influenced strongly by molecular structure. Bittermann and Goss (2017) modeled this resistance in Caco-2 cell monolayers for 135 chemicals, and the 95th percentile range of the estimates encompassed just a factor 6.6. We used the geometric mean of this dataset, 670000 s cm⁻¹ or 19000 h m⁻¹, took the inverse to obtain the permeation coefficient, and multiplied by a factor of 3 to correct for the lesser thickness of the gill epithelium (6 μm) compared to Caco-2 cells (14-20 μm) (Hughes, 1984; Tan et al., 2018).

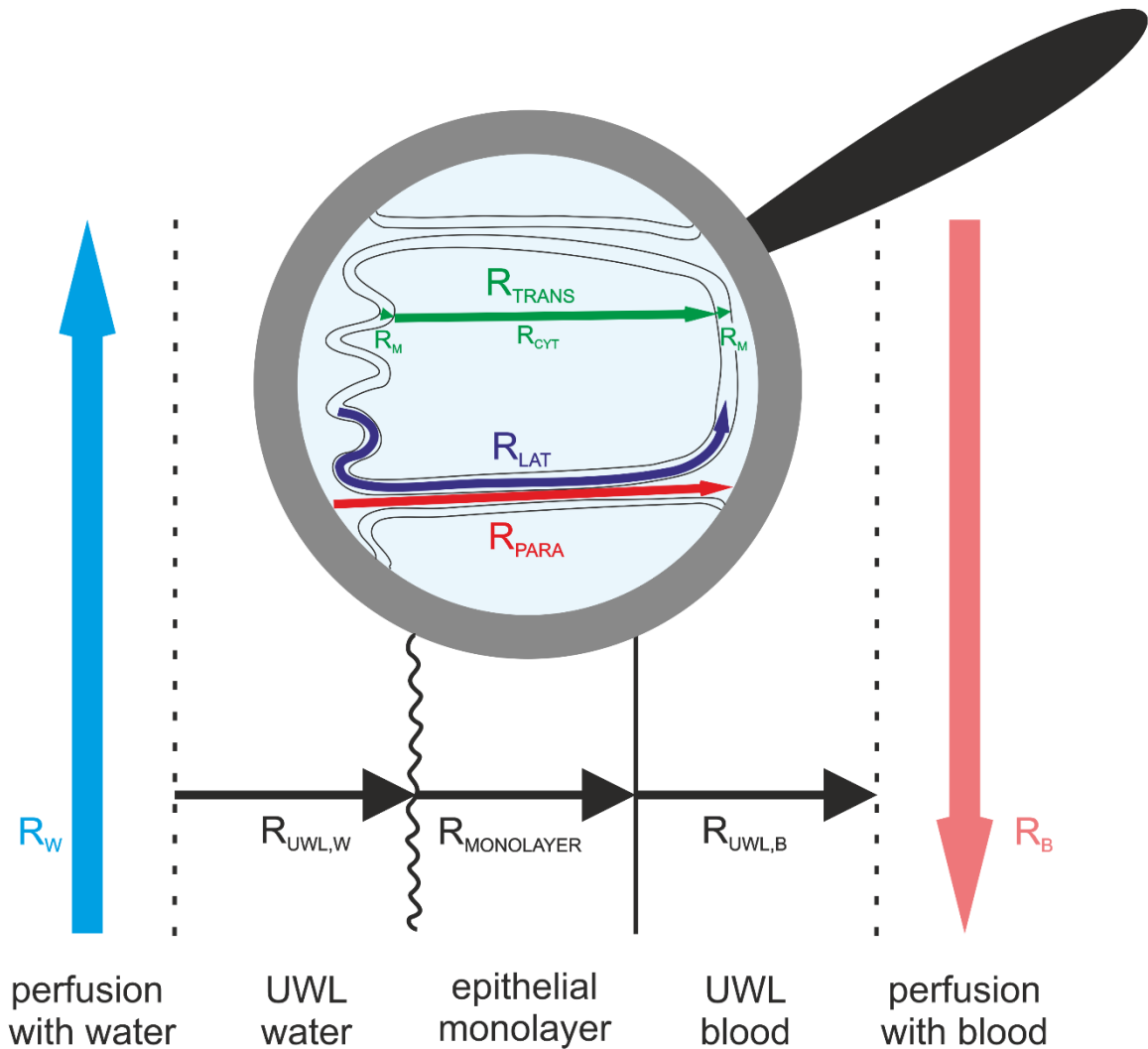
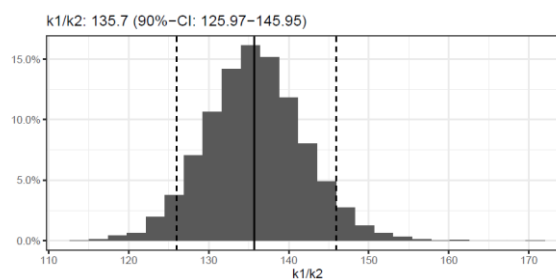
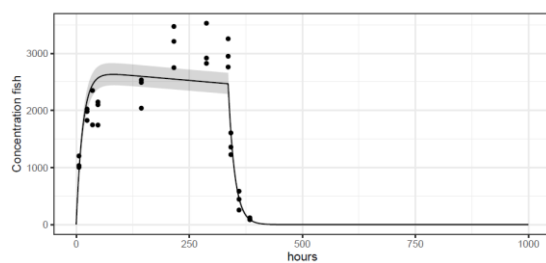


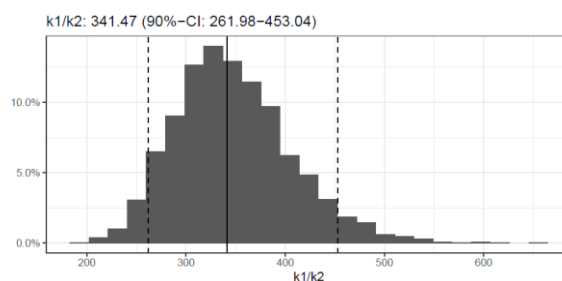
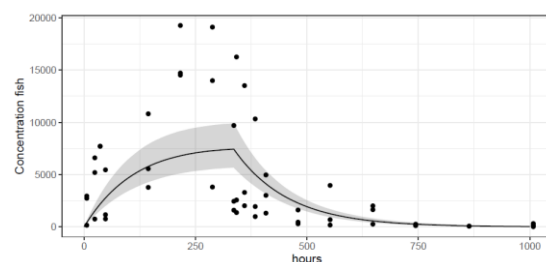
Figure S1: Illustration of the 4-resistance model used to describe surfactant exchange across the gills. R_W is the resistance from perfusion with water, $R_{UWL,W}$ is the resistance from diffusion through the laminar boundary layer (or unstirred water layer, UWL) of water at the outer gill surface, $R_{MONOLAYER}$ is the resistance of the epithelial monolayer, $R_{UWL,B}$ the resistance from diffusion through the laminar boundary layer on the inner side of the gill epithelium, and R_B is the resistance from perfusion with blood. $R_{MONOLAYER}$ is the result of three parallel resistance paths: the paracellular resistance R_{PARA} , the lateral resistance R_{LAT} , and the transcellular resistance R_{TRANS} . R_{TRANS} can further be subdivided into three resistances in series: the apical and basolateral membrane resistances R_M , and the resistance from diffusion through the cytosol R_{CYT} . We assume all aqueous resistances and lateral permeation to be insignificant (see the manuscript and Text S1), which leaves 4 resistances: R_W , R_{PARA} , R_M , R_B .

MIX1, pH = 7.6

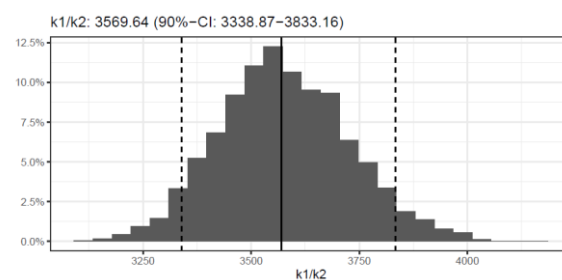
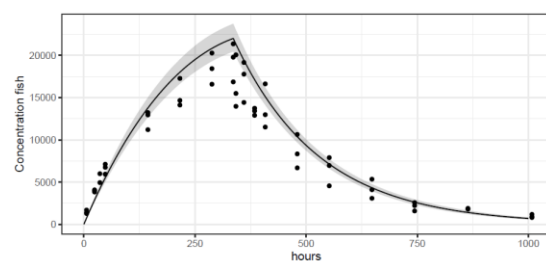
T10



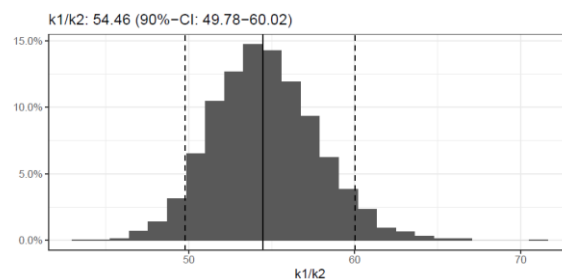
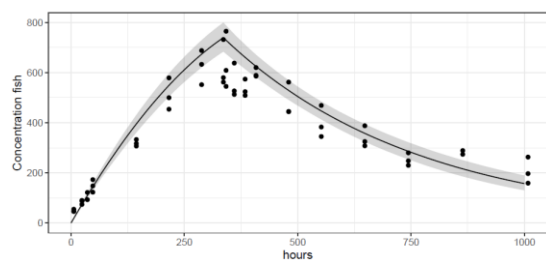
P12



T13



Q14



P16

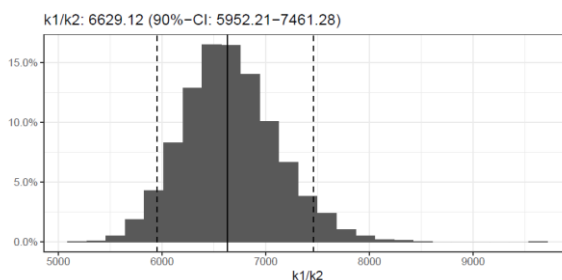
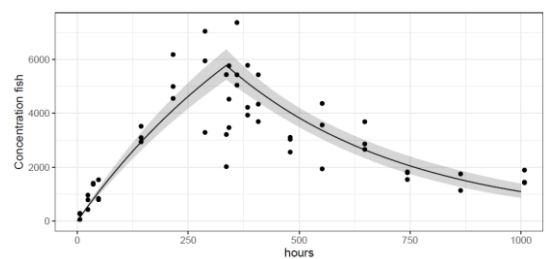
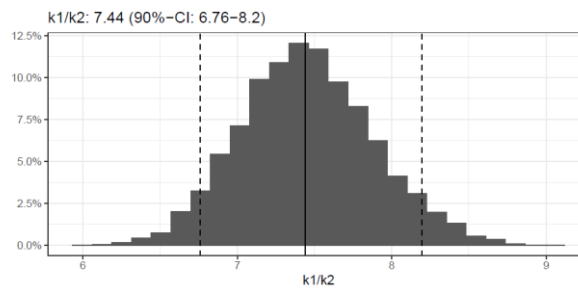
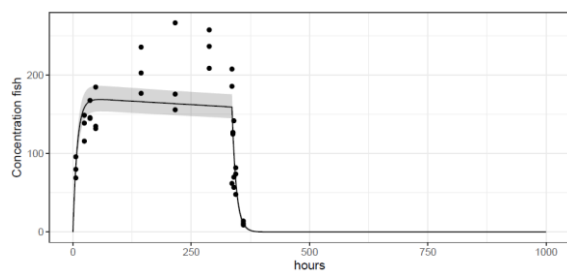


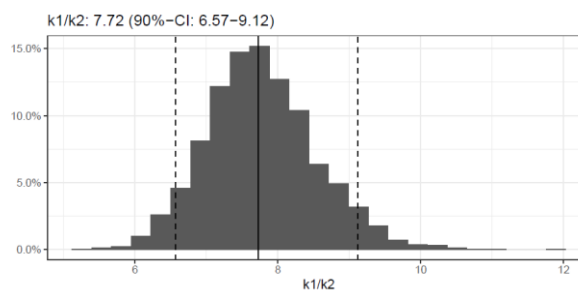
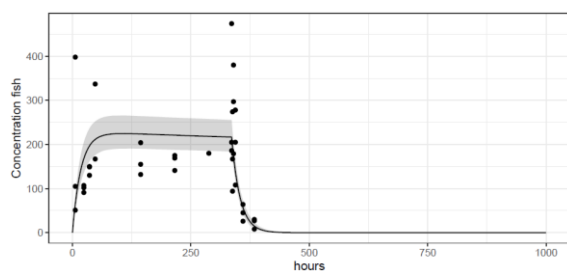
Figure S2: Fit of model to observations for cationic surfactants, see Table S3. The shaded area (left panel) shows the 90% credible region for the model-based concentration in water/fish over time.

MIX1pH, pH = 6.2

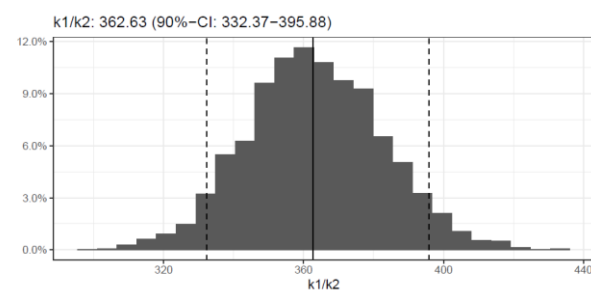
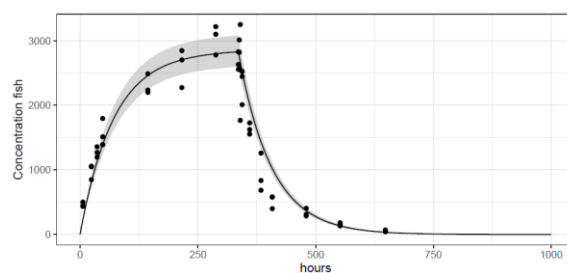
T10



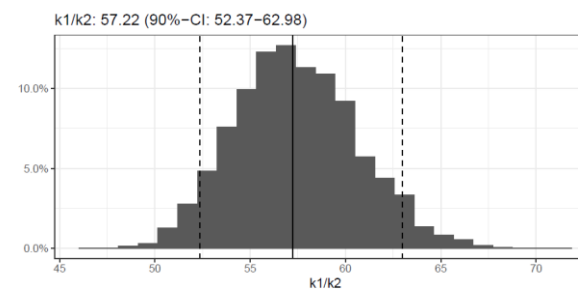
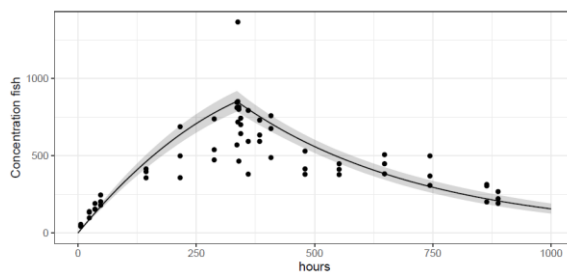
P12



T13



Q14



P16

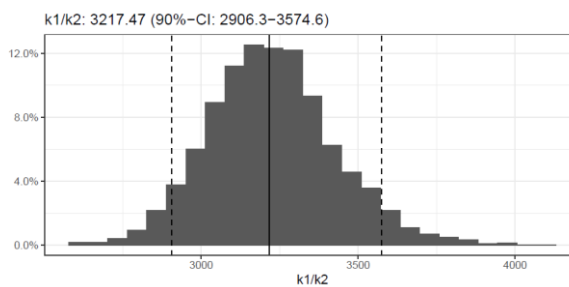
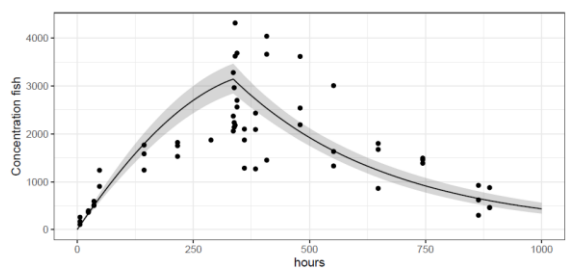
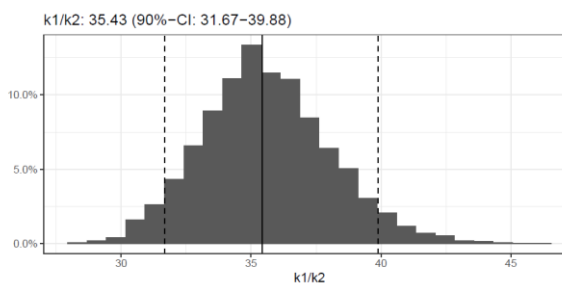
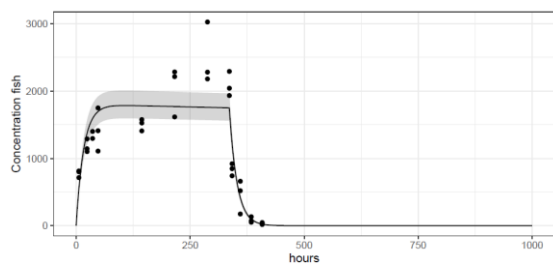


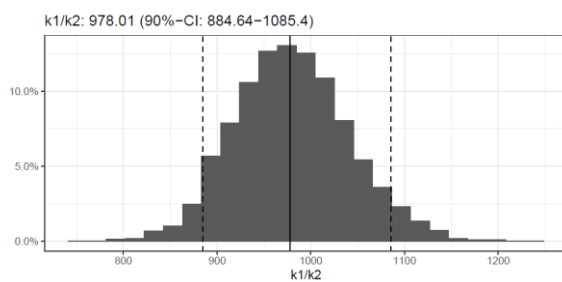
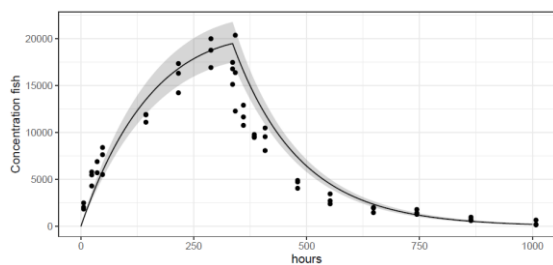
Figure S2 (continued)

MIX1, pH = 7.6

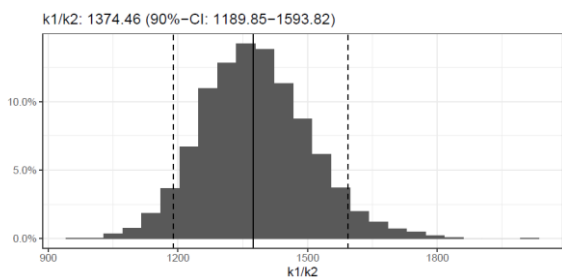
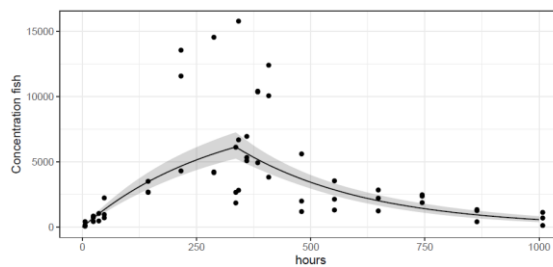
T9



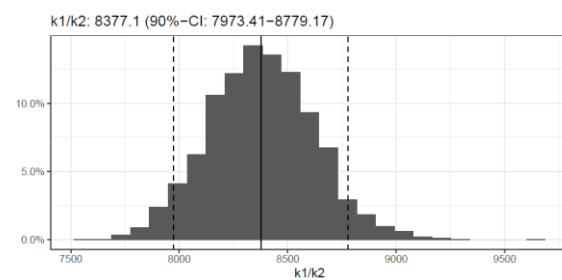
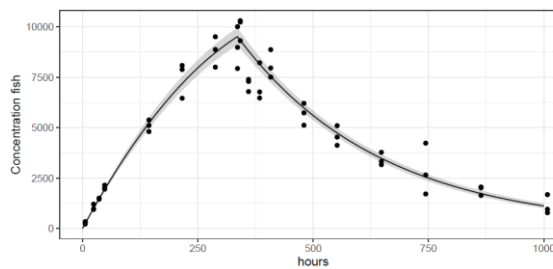
S12



P13



T14



S16

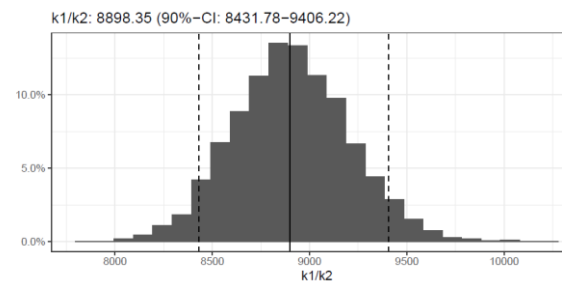
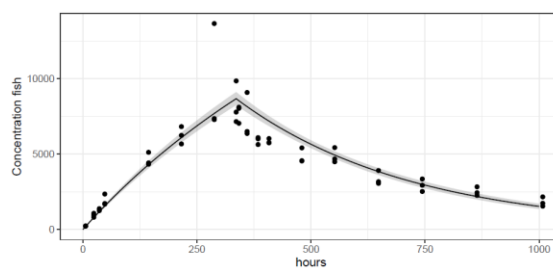


Figure S2 (continued)

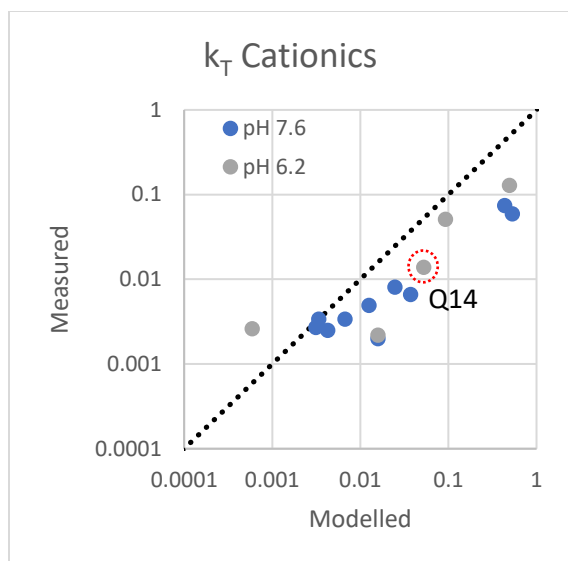


Table S1: Selected nonionic surfactants with tonnage >1000/y in the EU.

Tonnage (y ⁻¹)	CAS	Chain length range	Substance name (with hyperlink to REACH dossier)	Surface tension (mN/m)	REACH dossier #
100.000-1.000.000	68439-50-9	C12-C14	Alcohols, C12-14, ethoxylated (1 - 2.5 moles ethoxylated)	41.9	16040
10.000-100.000	160901-19-9	C12-13	Alcohols, C12-13, branched and linear, ethoxylated	26.0	15818
10.000-100.000	68439-49-6	C16-18	Alcohols, C16-18, ethoxylated	67.5	13418
10.000-100.000	68515-73-1	C8-10	D-Glucopyranose, oligomers, decyl octyl glycosides	29-36	14947
10.000-100.000	110615-47-9	C10-16	D-Glucopyranose, oligomeric, C10-16-alkyl glycosides	29.5	14407
1.000-10.000		C12-14	Alcohols, C12-14 (even-numbered), ethoxylated, magnesium salts, < 2.5 mol EO	29.8	5619
1.000-10.000	68920-66-1	C16-18	Alcohols, C16-18 and C18-unsatd., ethoxylated		15961
1.000-10.000	71060-57-6	C8-10	Alcohols, C8-10, ethoxylated	32.6	33685
1.000-10.000	1338-41-6		Sorbitan stearate		15165

Table S2: Selected zwitterionic surfactants with tonnage >1000/y in the EU.

Tonnage (y ⁻¹)	CAS	Chain length range	Substance name (with hyperlink to REACH dossier)	Surface tension (mN/m)	REACH dossier #
1.000-10.000	66455-29-6	C12-14	Betaines, C12-14 (even numbered)-alkyldimethyl	36.1	14910
1.000-10.000	3332-27-2	C14	N,N-dimethyltetradecylamine N-oxide	32.4	14677
1.000-10.000	1471314-81-4	C12-18	3-C12-18-(even numbered)-alkylamido-N,N-dimethylpropan-1-amino oxide	35	14163

Table S3: k_U , k_T and BCF for cationic surfactants, recalculated from the raw data in Kierkegaard et al. (2021) using the Bayesian model described in Ribbenstedt et al. (2022). The 95% confidence interval is provided in brackets. §

	Uptake rate constant (k_U , L kg ⁻¹ h ⁻¹)	Measured total elimination rate constant (k_T , h ⁻¹)	BCF (k_U/k_T , L kg ⁻¹)
MIX1 (pH = 7.6)			
T10	9.4 (8.2-10.8)	0.069 (0.064-0.075)	136 (124-148)
P12	2.8 (1.9-4.3)	0.0082 (0.0068-0.0096)	341 (250-481)
T13	18.6 (16.7-20.9)	0.0052 (0.0048-0.0056)	3570 (3300-3890)
Q14	0.127 (0.112-0.143)	0.0023 (0.0020-0.0027)	54 (49-61)
P16	16.5 (14.2-19.3)	0.0025 (0.0020-0.0030)	6630 (5830-7640)
MIX1pH (pH = 6.2)			
T10	0.83 (0.68-1.01)	0.111 (0.097-0.126)	7.4 (6.6-8.3)
P12	0.43 (0.31-0.58)	0.056 (0.045-0.067)	7.7 (6.4-9.4)
T13	5.1 (4.4-5.9)	0.0142 (0.0132—0.0151)	363 (326-402)
Q14	0.146 (0.128-0.166)	0.0026 (0.0022-0.0030)	57 (52-64)
P16	9.6 (8.1-11.2)	0.0030 (0.0025-0.0035)	3220 (2860-3660)
MIX2 (pH = 7.6)			
T9	2.1 (1.8-2.6)	0.060 (0.055-0.065)	35 (31-41)
S12	6.6 (5.6-7.8)	0.0068 (0.0062-0.0073)	978 (867-1110)
P13	4.8 (3.8-6.3)	0.0035 (0.0028-0.0043)	1370 (1150-1650)
T14	27 (25-29)	0.0032 (0.0030-0.0034)	8380 (7910-8880)
S16	23 (21-25)	0.0026 (0.0024-0.0028)	8900 (8330-9520)

§ Figure S2, left panel, shows the fit of the Bayesian model (as applied previously to anionic surfactant BCF studies reported in Ribbenstedt et al. (2022)) to the concentrations in fish from the bioconcentration experiments with cationic surfactants in Kierkegaard et al. (2021). The grey margin around the curve indicates the 95% confidence interval. The right panel shows the distribution of the modeled BCF in L kg⁻¹.

References

- Arnot, J. A.; Gobas, F. A. P. C. A food web bioaccumulation model for organic chemicals in aquatic ecosystems. *Environ. Toxicol. Chem.* **2004**, *23*, 2343-2355.
- Bertelsen, S. L.; Hoffman, A. D.; Gallinat, C. A.; Elonen, C. M.; Nichols, J. W. Evaluation of log K_{ow} and tissue lipid content as predictors of chemical partitioning to fish tissues. *Environ. Toxicol. Chem.* **1998**, *17*, 1447-1455.
- Bittermann, K.; Goss, K.-U. Predicting apparent passive permeability of Caco-2 and MDCK cell-monolayers: A mechanistic model. *PLoS ONE* **2017**, *12*, e0190319.
- Dong, H.; Lu, G.; Wang, X.; Zhang, P.; Yang, H.; Yan, Z.; Liu, J.; Jiang, R. Tissue specific accumulation, depuration and effects of perfluorooctanoic acid on fish: Influences of aqueous pH and sex. *Sci. Total Environ.* **2023**, *861*, 160567.
- Ebert, A.; Hanneschlaeger, C.; Goss, K. U.; Pohl, P. Passive permeability of planar lipid bilayers to organic anions. *Biophys. J.* **2018**, *115*, 1931-1941.
- Ebert, A.; Allendorf, F.; Berger, U.; Goss, K.-U.; Ulrich, N. Membrane/water partitioning and permeabilities of perfluoroalkyl acids and four of their alternatives and the effects on toxicokinetic behavior. *Environ. Sci. Technol.* **2020**, *54*, 5051-5061.
- Eckert, F.; Klamt, A. Fast solvent screening via quantum chemistry: COSMO-RS approach. *AIChE J.* **2002**, *48*, 369-385.
- Endo, S.; Escher, B. I.; Goss, K.-U. Capacities of membrane lipids to accumulate neutral organic chemicals. *Environ. Sci. Technol.* **2011**, *45*, 5912-5921.
- Erickson, R. J.; McKim, J. M.; Lien, G. J.; Hoffman, A. D.; Batterman, S. L. Uptake and elimination of ionizable organic chemicals at fish gills: I. Model formulation, parameterization, and behavior. *Environ. Toxicol. Chem.* **2006**, *25*, 1512-1521.
- Hughes, G. M. General anatomy of the gills. In Hoar, W. S.; Randall, D. J., eds, *Fish Physiology*, Vol XA. Academic, New York, 1984, pp 1-72.
- Kierkegaard, A.; Sundbom, M.; Yuan, B.; Armitage, J.M.; Arnot, J.A.; Droge, S.T.J.; McLachlan, M.S. Bioconcentration of several series of cationic surfactants in rainbow trout. *Environ. Sci. Technol.* **2021**, *55*, 8888-8897.
- Lomize, A. L.; Pogozheva, I. D. Physics-based method for modeling passive membrane permeability and translocation pathways of bioactive molecules. *J. Chem. Inf. Model.* **2019**, *59*, 3198-3213.
- Missner, A.; Pohl, P. 110 years of the Meyer-Overton rule: Predicting membrane permeability of gases and other small compounds. *Chem. Phys. Chem.* **2009**, *10*, 1405-1415.
- Orbach, E.; Finkelstein, A. The nonelectrolyte permeability of planar lipid bilayer membranes. *J. Gen. Physiol.* **1980**, *75*, 427-436.

Ribbenstedt, A.; Armitage, J.; Günther, F.; Arnot, J.; Droge, S.; McLachlan, M. S. In vivo bioconcentration of 10 anionic surfactants in rainbow trout explained by in vitro data on partitioning and S9 clearance. *Environ. Sci. Technol.* **2022**, *56*, 6305-6314.

Tan, H.-Y.; Trier, S.; Rahbek, U. L.; Dufva, M.; Kutter, J. P.; Andresen, T. L. A multi-chamber microfluidic intestinal barrier model using Caco-2 cells for drug transport studies. *PLoS ONE* **2018**, *13*, e0197101.

Walter, A.; Gutknecht, J. Permeability of small nonelectrolytes through lipid bilayer membranes. *J. Membr. Biol.* **1986**, *90*, 207-217.